Turkish Computational and Theoretical Chemistry

Turkish Comp Theo Chem (TC&TC)

Volume(Issue): 9(2) – Year: 2025 – Pages: 125-136

e-ISSN: 2602-3237

https://doi.org/10.33435/tcandtc.1672804

Received: 09.04.2024 ***Accepted***: 28.04.2025 *Research Article*

INVESTIGATION OF STRUCTURAL PROPERTIES OF FERROCENE-DERIVED CHALCONE COMPOUNDS

Gamze Tüzün[1], Koray Sayın

Deparment of Chemistry, Science Faculty, Sivas Cumhuriyet University, Sivas, 58140, Turkey

Abstract: Ferrocene derived chalcone compounds were completed at M06-2X/6-31+G(d)(LANL2DZ) level in water phase. Structural properties (geometric structure, bond lengths and angles), spectral electronic properties and nonlinear optical properties (NLO) of the relevant compounds were examined. Geometric parameters of these compounds and their electronic structures were reported. HOMO-LUMO energy gap (6.35-6.77 eV) indicated high stability of the compounds, while MEP maps revealed that carbonyl oxygens have biological interaction potential. IR spectra of ferrocene derived chalcone compounds were calculated in water phase. Absorption bands were observed between 190-285 nm in UV-Vis spectrum. In NLO analysis, FC9 and FC10 compounds were determined to have high second-order polarizability (βtot) values (FC10: 1892.80 a.u.), and FC6 compound had the highest dipole moment (1.98 Debye). Overall, the calculated molecular parameters indicate that ferrocene-derived chalcone compounds have the potential to interact with biological and chemical systems. These findings provide a theoretical basis for further experimental studies and are suggested to be evaluated in pharmaceutical and biotechnological applications.

Keywords: DFT, Ferrocene, Chalcone, HOMO-LUMO, NLO, Spectroscopy

Graphical Abstract:

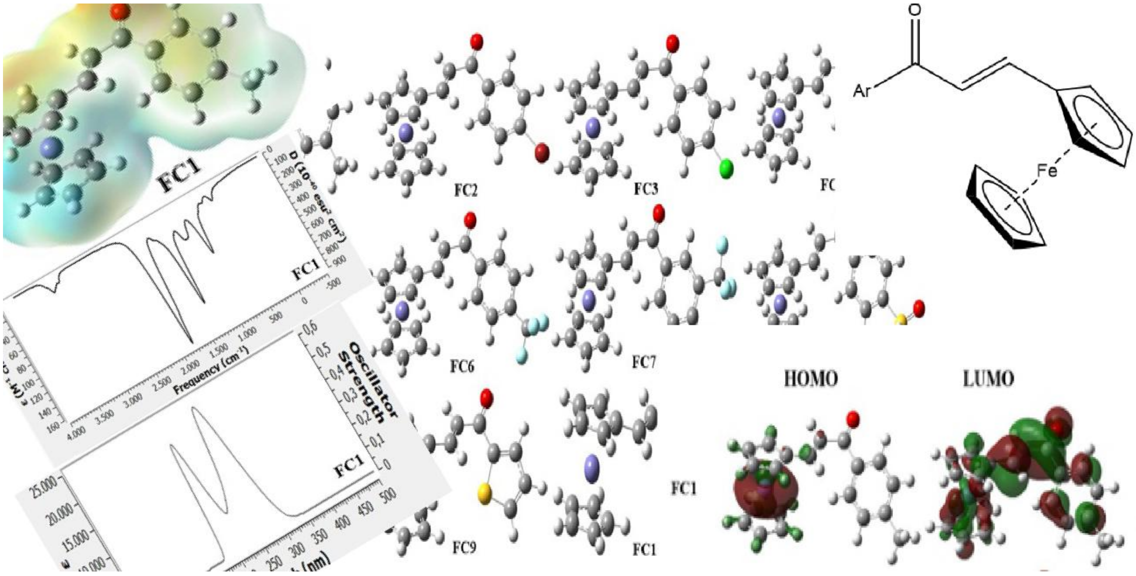

1. Introduction

Ferrocene-derived compounds occupy an important place in the field of organometallic chemistry. Kealy and Pauson discovered the ferrocene molecule in 1951. It is a metalorganic compound that has a sandwich-like structure, with two

---

[1] Corresponding Authors

e-mail: gamzekekul@gmail.com

cyclopentadienyl (Cp) rings around an iron (Fe) core [1]. Ferrocene has a number of qualities that are a result of its unusual structure, including high stability, chemical adaptability, and the capacity to be modified for environmental purposes [2]. As a consequence, ferrocene has been used in a variety of fields, including drug design, catalysis, material sciences, and sensor creation. Chalcones are chemical compounds that are generated from flavonoids. They are made up of aromatic rings that are connected by an α, β-unsaturated carbonyl group. These molecules are often found in nature and are of high interest because of their biological functions and chemical reactivity [3]. Chalcone derivatives are being researched as possible pharmacological agents because they have a wide range of biological activities, including anticancer, antibacterial, antioxidant, and anti-inflammatory effects [4]. These chemicals have been shown to be especially efficient in inhibiting cell growth and as specific enzyme inhibitors in the literature.

By combining the capabilities of organic and metalloorganic chemistry, the chemical combination of ferrocene and chalcone makes it possible to construct new molecular patterns. By combining the unique redox characteristics of ferrocene with the biological activities of chalcone, this combination offers a wide range of applications that are both adaptable and focused. In recent years, the anticancer characteristics of ferrocene-derived chalcone compounds and their potential as Hsp90 inhibitors have been an interesting field of investigation [5]. According to the literature, these compounds have been shown to have cytotoxic effects on certain cancer cell lines and to have the potential to bind to certain protein targets.

Computational chemistry is an incredibly useful technique for understanding and producing molecules at the molecular level. Quantum chemistry approaches (such DFT and HF) and molecular dynamics simulations are useful for analyzing the electronic structures, energy levels, reactivity characteristics, and interactions of ferrocene-derived chalcone compounds with biological targets. When these methodologies are paired with experimental data, they offer a solid foundation for the creation of pharmacological compounds that are more effective and selective [6]. The goal of this work is to use computational chemistry tools to analyze the molecular structure and biological consequences of chalcone molecules that are produced from ferrocene. Given the present understanding in the literature, the ways in which molecular design methodologies and computational approaches help to anticipate the activities of these compounds and their prospective therapeutic uses will be stressed [7]. In this setting, the goal is for the data that are collected to provide insight into future pharmaceutical development procedures.

The aim of this study is to investigate the structural, electronic and optical properties of ferrocene derived chalcone compounds using density functional theory (DFT). It is aimed to determine the molecular orbitals, electrostatic potential distributions and biological interaction potentials of these compounds through calculations. In this way, it is aimed to contribute to the design of new and effective compounds for pharmaceutical and optoelectronic applications.

2. Computational Method

In this study, quantum chemistry calculations of ferrocene-derived chalcone compounds were performed using GaussView 6.0 and Gaussian 16 software [8,9]. For the calculations, the M06-2X functional and the 6-31+G(d) basis set (for main element atoms) and the LANL2DZ basis set (for iron atoms) were combined. The M06-2X functional was preferred due to its high accuracy in the energy calculations of organic and metalloorganic systems, in the determination of molecular properties and in compounds containing transition metals. While the geometry optimization included a full optimization for all molecules, molecular properties such as HOMO-LUMO energy levels, ionization potential (I), electron affinity (A), chemical hardness (η), chemical potential (μ), electronegativity (χ), electrophilicity index (ω) and dipole moment were calculated following these steps [10,11]. No symmetry restrictions were applied in the optimization processes and all calculations were performed in the gas phase. In addition, ESP (electrostatic potential) maps, IR vibration frequencies and NMR chemical shift values of the molecules were obtained. HOMO-LUMO energy levels and other related molecular parameters were calculated using the following formulas:

$$\chi = -\left(\frac{\partial \mathrm{E}}{\partial \mathrm{N}}\right)_{\upsilon(r)} = \frac{1}{2}(I + A) \cong \frac{1}{2}(E_{HOMO} + E_{LUMO})$$

$$\eta = -\left(\frac{\partial^2 \mathrm{E}}{\partial \mathrm{N}^2}\right)_{\upsilon(r)} = \frac{1}{2}(I - A) \cong -\frac{1}{2}(E_{HOMO} - E_{LUMO})$$

$$\sigma = 1/\eta \qquad \omega = \chi^2/2\eta \qquad \varepsilon = 1/\omega$$

GaussView 6 software was used to see and analyze the results of the calculations that were produced. ChemOffice was used to create drawings and structural designs of molecules.

These calculating techniques make it possible to assess experimental and theoretical data in a way that is consistent with finding molecular properties that are connected to biological activities. This provides a solid foundation for the investigation of the reactivity and stability of chalcone compounds that are generated from ferrocene. In particular, the computed molecular characteristics are a significant reference for predicting biological activities and designing novel derivatives.

3. Results and discussion

The chalcone compounds produced from ferrocene derivatives are among the remarkable structures in organometallic chemistry and stand out especially with their biological activities. The unique properties of these compounds combine both the metallic character of ferrocene and the wide biological spectrum of chalcones. Theoretical studies provide important information about the potential biological and industrial applications by providing a detailed understanding of the structural and electronic properties of these molecules [12,13]. In this context, understanding the chemical behavior and interaction mechanisms of ferrocene-derived chalcones constitutes an important step for the development of new and effective therapeutic agents.

Table 1 shows the groups attached to the R groups in ferrocenyl compounds at 5 different positions. By connecting these different groups, 10 FC series molecules were obtained. In Figure 1, the optimized versions of these structures are given.

Table 1. R groups in ferrocenyl compounds

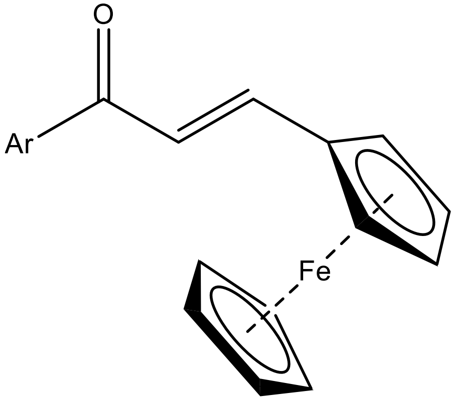

Ferrocenyl_Chalcone Derivative (**FC**)

Compounds	**Ar**	**Compounds**	**Ar**
FC1	4-CH_3-C_6H_4	**FC6**	4-CF_3-C_6H_4
FC2	4-Br-C_6H_4	**FC7**	3-CF_3-4-Cl-C_6H_4
FC3	4-Cl-C_6H_4	**FC8**	4- SO_2CH_3-C_6H_4
FC4	3-OCF_3-C_6H_4	**FC9**	C_4H_4S
FC5	3-CF_3-C_6H_4	**FC10**	C_4H_4O

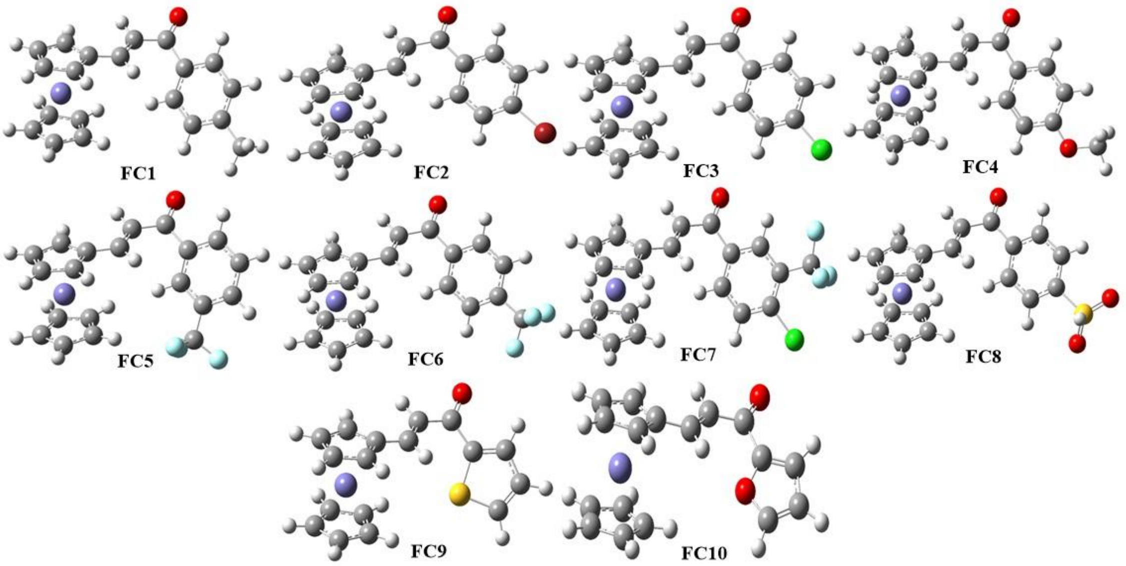

Figure1. Representations of optimize structure of FC series molecules

Table 2 contains bond lengths (Å) and bond angles (degrees) data for molecules of the FC series. This table allows detailed examination of the geometric structure of molecules. Bond lengths indicate the distances of atomic connections between molecules, while bond angles indicate the orientations of these connections in space. Such geometric parameters are critical for understanding the structural stability, reactivity, and potential interaction mechanisms of molecules.

The molecular orbital properties of ferrocene-derived chalcone compounds were analyzed by examining the HOMO and LUMO orbitals obtained as a result of quantum chemistry calculations in Figure 2 and Table 3. Molecular orbital energy levels were used to understand the electronic properties and chemical reactivity trends of the compounds. The HOMO-LUMO energy difference (ΔE) was used as a basic parameter to evaluate the electronic transitions and stabilities of the compounds [14].

Table 2. Value of Bond lengths (Å) and Bond angles (deg.) of FC series molecules

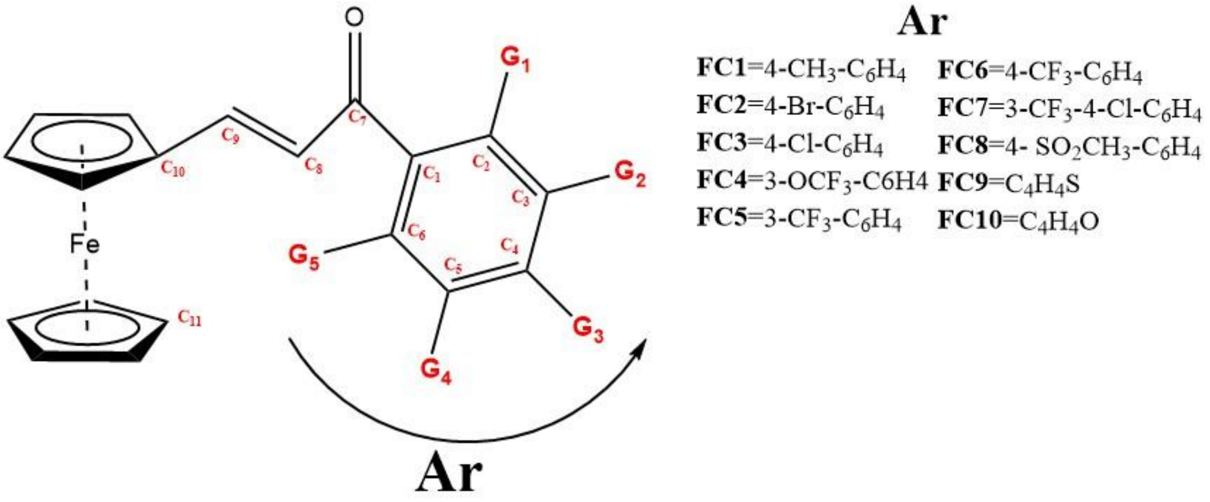

	FC1	FC2	FC3	FC4	FC5	FC6	FC7	FC8	FC9	FC10

Bond lengths (Å)										
C_{10}-Fe	2.13	2.13	2.13	2.13	2.13	2.13	2.13	2.13	2.13	2.13
C_{11}-Fe	2.13	2.13	2.13	2.13	2.13	2.13	2.13	2.13	2.13	2.13
C_9=R_8	1.34	1.34	1.34	1.34	1.35	1.34	1.34	1.35	1.34	1.34
C_7=O	1.22	1.22	1.22	1.22	1.22	1.22	1.22	1.22	1.22	1.22
C_3-G_2	-	-	-	-	-	-	1.51	-	-	-
C_4-G3	1.51	1.89	1.74	1.36	-	1.50	1.73	1.78	-	-
C_5-G_4	-	-	-	-	1.50	-	-	-	-	-
Bond angles (deg.)										
C_4-C_3-G_2	-	-	-	-	-	-	121.13	-	-	-
C_4-C_5-G_4	-	-	-	-	120.92	-	-	-	-	-
C_5-C_4-G_3	121.34	119.34	119.30	115.77	-	120.91	118.32	118.84	-	-
C_8-C_7-C_1	120.25	120.19	120.17	120.15	120.04	120.24	120.16	120.34	120.57	121.94
C_{10}-C_9-C_8	125.48	125.49	125.45	125.45	125.67	125.47	125.48	125.51	125.35	124.75
C_{11}-Fe-C_{10}	112.73	112.97	113.32	113.23	112.82	112.98	112.97	125.51	111.58	109.75
Dihedral angles (deg.)										
Fe-C_{10}-C_9-C_7	125.51	105.44	106.40	106.87	102.39	104.78	105.51	103.62	104.82	103.99
C_{10}-C_8-C_1-C_6	44.40	44.66	45.04	43.71	42.53	45.42	44.54	45.45	-	-
C_9-C_7-C_1-C_2	-137.75	-137.32	-136.96	-138.98	-138.76	-135.91	-117.68	-136.05	-131.09	-160.99

Table 3. The molecular orbital properties value of ferrocene-derived chalcone compounds (eV)

	E_{HOMO}	**E_{LUMO}**	**I**	**A**	**ΔE**	**η**	**μ**	**χ**	**PA**	**ω**	**ε**	**dipol**	**Energy**
M06-2X/6-31+G(d)(LANL2DZ)													
FC1	-7.7167	-0.9821	7.7167	0.9821	6.7346	3.3673	0.2970	4.3494	-4.3494	2.8089	0.3560	4.4987	-26420.8077
FC2	-7.8628	-1.2504	7.8628	1.2504	6.6124	3.3062	0.3025	4.5566	-4.5566	3.1399	0.3185	4.4351	-95310.3322
FC3	-7.8579	-1.2229	7.8579	1.2229	6.6350	3.3175	0.3014	4.5404	-4.5404	3.1070	0.3219	4.4060	-37858.0211
FC4	-7.6848	-0.9170	7.6848	0.9170	6.7678	3.3839	0.2955	4.3009	-4.3009	2.7332	0.3659	3.7584	-28466.5807
FC5	-7.8350	-1.3402	7.8350	1.3402	6.4949	3.2474	0.3079	4.5876	-4.5876	3.2404	0.3086	2.6308	-34521.2408
FC6	-7.9344	-1.4052	7.9344	1.4052	6.5292	3.2646	0.3063	4.6698	-4.6698	3.3399	0.2994	5.0414	-34521.2048
FC7	-8.0078	-1.4966	8.0078	1.4966	6.5112	3.2556	0.3072	4.7522	-4.7522	3.4684	0.2883	7.0241	-47026.8496
FC8	-8.0288	-1.6722	8.0288	1.6722	6.3566	3.1783	0.3146	4.8505	-4.8505	3.7012	0.2702	7.4672	-40276.6711
FC9	-7.7439	-1.1761	7.7439	1.1761	6.5678	3.2839	0.3045	4.4600	-4.4600	3.0286	0.3302	4.0549	-34081.3322
FC10	-7.6884	-1.1413	7.6884	1.1413	6.5471	3.2736	0.3055	4.4148	-4.4148	2.9770	0.3359	4.1564	-25292.7966

HOMO and LUMO orbital visualizations were made using GaussView 6 software. The HOMO orbital represents the donor electron capacity of the molecule, while the LUMO orbital represents the acceptor electron capacity [15]. The high energy level of the HOMO orbital determines the ionization potential of the molecule; the low energy level of the LUMO level determines the electron affinity.

Contour plots of the HOMO and LUMO orbitals were used to visualize how the orbitals are localized on the molecule. In these graphs, HOMO orbitals are generally concentrated in π-bonds, while LUMO orbitals indicate regions where electrons can be accepted into the molecule [16].

The color scale used in contour graphs made it possible to distinguish positive and negative phases. This plays a critical role in understanding the electronic distributions and potential reactivity regions of molecules.

Molecular orbital energy diagrams clearly show the relative positions and energy differences of HOMO-LUMO energy levels [17]. These diagrams provide important information about the stability and chemical reactivity of the molecule. Especially in ferrocene-derived chalcone compounds, it was observed that HOMO orbitals were localized to the ferrocene unit and LUMO orbitals were localized to the chalcone group.

This situation shows that the electronic properties of the compounds are distributed between metalloorganic and organic components and that these two units work synergistically.

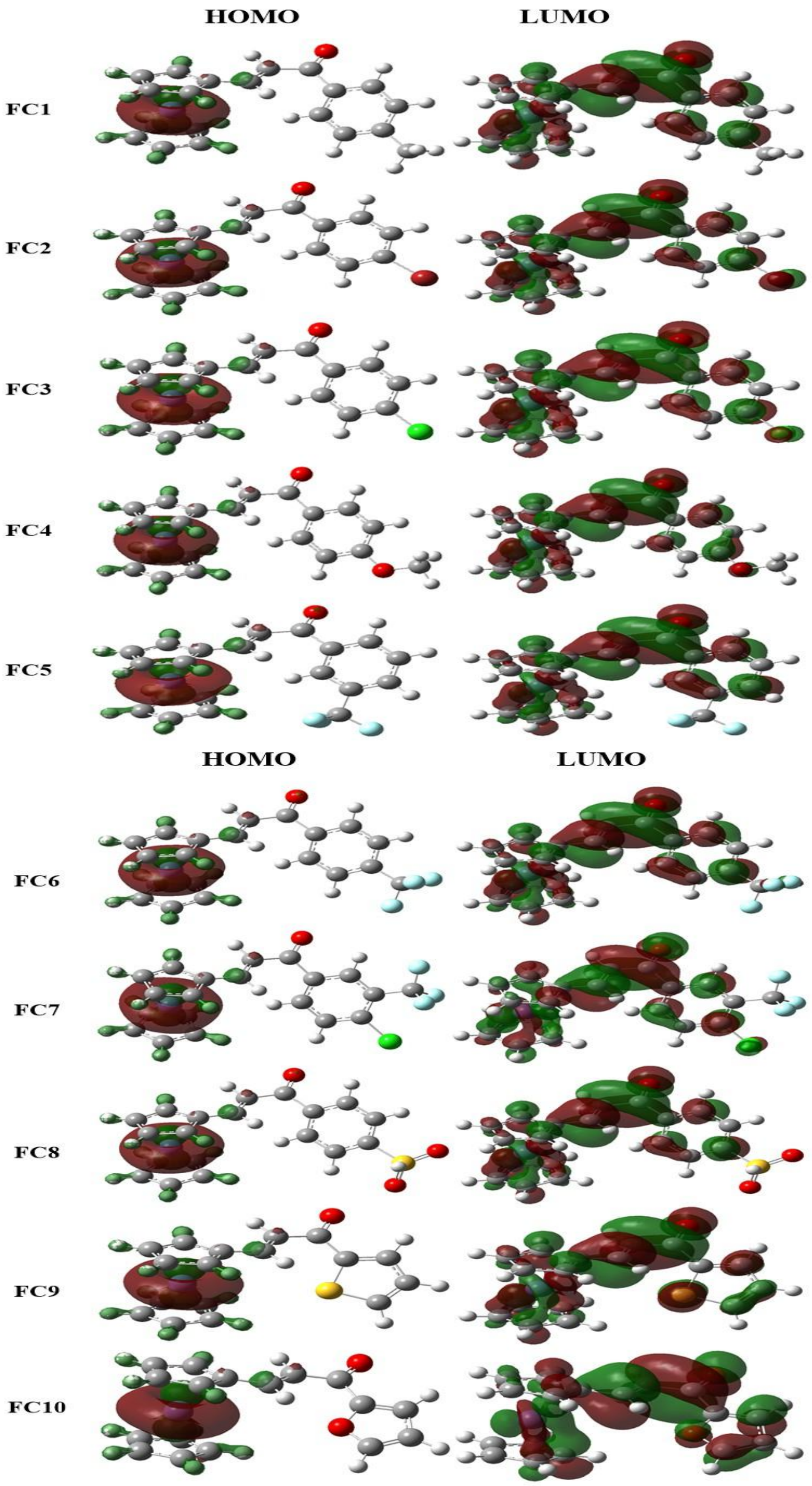

Figure 2. Representations of HOMO and LUMO of FC series molecules

Molecular electrostatic potential (MEP) maps were generated for ferrocene-derived chalcone compounds in order to show the electrostatic characteristics and reactivity zones of the molecules in Figure 3. MEP maps show how the electrostatic charge is distributed on the surface of a molecule. This information may be used to identify the nucleophilic and electrophilic areas of the molecule. The GaussView 6 interface was used to show the findings generated from quantum chemistry calculations that were performed using Gaussian 16 software. MEP maps are drawn on the optimized molecular geometry and use color coding to show the electrostatic potential values of various locations on the surface of the molecule. Red areas show the negative potential and suggest areas that are open to nucleophilic interactions (areas that are packed with electrons) [18]. The blue areas show the positive potential and suggest regions that are open to electrophilic interactions (regions that attract electrons). zones with neutral or low electrostatic potential are represented by green and yellow zones [19]. MEP maps show that the metallic iron core in the ferrocene unit is often considered a neutral area with a reduced electrostatic potential. The carbonyl oxygen atom of the chalcone group is a region with negative potential and exhibits strong nucleophilic characteristics, making it stand out. Moreover, the π-electron density in the ferrocene ring and the α,β-unsaturated carbonyl group in the chalcone group produce key nucleophilic and electrophilic areas for intermolecular interactions.

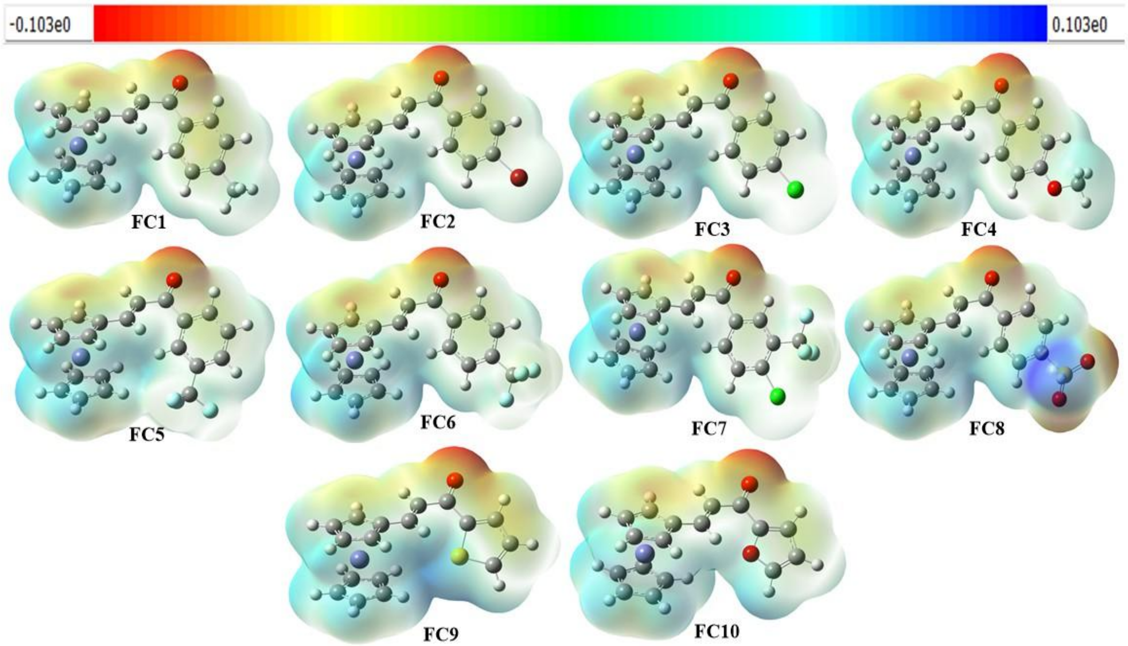

Figure 3. Representations of ESP of FC series molecules

These maps are a useful resource for predicting interactions between molecules or between molecules and biological targets [20]. For instance, examining the electrostatic compatibility of these compounds with their biological targets yields important information that may be used to assess their potential inhibitory characteristics.

The investigations of MEP maps help to provide a more thorough knowledge of the biological and chemical reactivity characteristics of compounds. In particular, electrostatic variations on the molecular surface have been a crucial aid in understanding the binding affinities of these substances with various enzymes or proteins.

The table contains IR spectrum data for FC1-FC10 molecules in Figure S1 and Table 4. These data represent the characteristic vibration modes of the molecules and the frequencies of these modes. It has been observed that different vibrations occur in each vibration mode occurring in the molecule. C-H vibrations (*ν*C-H), values are generally between 3132-3136 cm^{-1} and show a small change. This region represents the stretching vibrations of C-H bonds and is usually observed in aromatic rings. The narrow range of values indicates that C-H bonds have a similar structure or that environmental effects are limited.

Carbonyl vibrations (*ν*C=O), These vibrations observed between 1712-1693 cm^{-1} represent the stretching vibrations of the carbonyl (C=O) group. The fact that the frequencies differ slightly indicates that the carbonyl group may have different resonance structures due to environmental effects or the molecule.

C=C vibrations (*ν*C=C), these values varying between 1466-1345 cm⁻¹ indicate the stretching vibrations of C=C double bonds. The change in these values may be due to the electronic effects of the groups to which the double bond is attached.

C-C vibrations (*ν*C-C), these vibrations varying between 1304-1245 cm⁻¹ represent the characteristic frequencies of C-C bonds. The small differences between the frequencies vary depending on the bond environment of the carbon to which the C atom is attached.

Table 4. IR spectrum value for FC1-FC10 molecules

Labeling	FC1	FC2	FC3	FC4	FC5	FC6	FC7	FC8	FC9	FC10
$\nu_{Cp(C\text{-}H)}$	3132	3134	3133	3133	3134	3133	3133	3133	3136	3135
$\nu_{C=O}$	1705	1708	1702	1702	1710	1711	1712	1712	1700	1693
$\nu_{C=C}$	1402	1466	1646	1612	1421	1467	1358	1380	1345	1367
$\nu_{C\text{-}C}$	1261	1258	1259	1302	1237	1261	1304	1261	1245	1297
$\nu_{Fe\text{-}C}$	433	407	427	406	435	424	432	419	408	412

Fe vibrations (*ν*Fe), these vibrations observed between 435-406 cm⁻¹ represent the vibration modes of bonds containing iron (Fe). The differences between the frequencies may depend on the position of ferrocene or similar groups in the structure.

As a result, IR spectrum data represent the vibration modes of different bond types of molecules. Small differences in frequencies may be due to electronic effects of groups in the molecular structure, steric interactions, or environmental factors between molecules. Changes in the C=O and C=C regions in particular can provide detailed information about the chemical environment of the bonds. Such data are very valuable for identifying functional groups in molecules and understanding structure-vibration relationships.

Table 5 shows the calculated UV-Vis absorption bands of various FC compounds at the M06-2X/6-31+G(d)(LANL2DZ) level. All UV-Vis spectra of ferrocene-based chalcone derivative molecules are given in Figure S2. When this table is examined in detail, the "Main Band" and "Other Band" columns show the wavelengths (in nm) of the two main absorption bands calculated for each compound. It is seen that the wavelengths are generally in the range of 190-285 nm, which is known to be a region commonly associated with π→π* or n→π* transitions [21]. Small wavelength variations between compounds are predicted to be due to differences in electronic structure or the width of conjugation. These data are important for understanding the electronic structure and light absorption properties of molecules and can be used in photochemical or biological applications [22].

Table 6. NLO parametres value of complexes

	FC1		**FC2**			**FC1**		**FC2**	
	a.u.	10su	a.u.	10su		a.u.	10su	a.u.	10su
α_{xx}	304.5608	4.5075 10^{-23}	316.7070	4.68726 10^{-23}	β_{xxx}	1296.6622	1.120 10^{-26}	974.5473	8.421 10^{-27}
α_{xy}	3.7569	5.5602 10^{-25}	4.4055	6.52015 10^{-25}	β_{yyy}	462.9651	4.000 10^{-27}	837.6746	7.238 10^{-27}
α_{yy}	243.2217	3.5997 10^{-23}	257.9951	3.81833 10^{-23}	β_{zzz}	-187.6024	-1.621 10^{-27}	13.6710	1.181 10^{-28}
α_{xz}	-1.1489	-1.7004 10^{-25}	-2.0734	-3.06863 10^{-25}	β_{xyy}	64.7404	5.594 10^{-28}	77.8777	6.729 10^{-28}
α_{yz}	-9.9992	-1.4799 10^{-24}	-7.4012	-1.09538 10^{-24}	β_{xxy}	-294.8888	-2.548 10^{-27}	-317.8461	-2.747 10^{-27}
α_{zz}	182.9053	2.7070 10^{-23}	184.1860	2.72595 10^{-23}	β_{xxz}	4.9751	4.299 10^{-29}	-71.0486	-6.139 10^{-28}
Δ_{α}	81.5353	1.206 10^{-23}	193.0359	2.85693 10^{-23}	β_{xzz}	-31.7908	-2.747 10^{-28}	-39.8478	-3.443 10^{-28}
μ_x	-0.8010	-1.185 10^{-25}	-1.3176	-1.9501 10^{-25}	β_{yzz}	-8.0362	-6.944 10^{-29}	21.4413	1.853 10^{-28}
μ_y	-1.3783	-2.040 10-^{25}	-1.0066	-1.4897 10^{-25}	β_{yyz}	-3.2597	-2.817 10^{-29}	-16.4121	-1.418 10^{-28}

μ_z	0.7689	$1.138\ 10^{-25}$	0.5435	$8.04327\ 10^{-26}$	β_{total}	1352.0481	$1.168\ 10^{-26}$	1150.5349	$9.942\ 10^{-27}$
μ_g	1.7699		1.7449						
	FC3		**FC4**			**FC3**		**FC4**	
	a.u.	10su	a.u.	10su		a.u.	10su	a.u.	10su
α_{xx}	305.8003	$4.52584\ 10^{-23}$	316.7878	$4.68846\ 10^{-23}$	β_{xxx}	1213.2583	$1.048\ 10^{-26}$	966.2248	$8.349\ 10^{-27}$
α_{xy}	3.2594	$4.82396\ 10^{-25}$	2.6002	$3.84827\ 10^{-25}$	β_{yyy}	681.5644	$5.889\ 10^{-27}$	778.9162	$6.731\ 10^{-27}$
α_{yy}	248.1978	$3.67333\ 10^{-23}$	248.5020	$3.67783\ 10^{-23}$	β_{zzz}	-147.7494	$-1.277\ 10^{-27}$	-261.3522	$-2.258\ 10^{-27}$
α_{xz}	-1.0128	$-1.49889\ 10^{-25}$	-1.1374	$-1.68329\ 10^{-25}$	β_{xyy}	104.5074	$9.030\ 10^{-28}$	147.4925	$1.274\ 10^{-27}$
α_{yz}	-8.9490	$-1.32446\ 10^{-24}$	-8.5966	$-1.27229\ 10^{-24}$	β_{xxy}	-322.7980	$-2.789\ 10^{-27}$	-332.8374	$-2.876\ 10^{-27}$
α_{zz}	179.2042	$2.65222\ 10^{-23}$	184.3912	$2.72899\ 10^{-23}$	β_{xxz}	-22.1196	$-1.911\ 10^{-28}$	2.4257	$2.096\ 10^{-29}$
Δ_α	185.7525	$2.74914\ 10^{-23}$	189.2967	$2.80159\ 10^{-23}$	β_{xzz}	-38.5961	$-3.335\ 10^{-28}$	51.3122	$4.434\ 10^{-28}$
μ_x	-1.4138	$-2.0924\ 10^{-25}$	-0.2000	$-2.9600\ 10^{-26}$	β_{yzz}	-5.0579	$-4.371\ 10^{-29}$	1.3296	$1.149\ 10^{-29}$
μ_y	-0.8391	$-1.2419\ 10^{-25}$	-1.2237	$-1.8110\ 10^{-25}$	β_{yyz}	-1.0435	$-9.017\ 10^{-30}$	20.6121	$1.781\ 10^{-28}$
μ_z	0.5496	$8.1346\ 10^{-26}$	0.7980	$1.18103\ 10^{-25}$	β_{total}	1338.1315	$1.156\ 10^{-26}$	1270.5360	$1.098\ 10^{-26}$
μ_g	1.7335		1.4745						
	FC5		**FC6**			**FC5**		**FC6**	
	a.u.	10su	a.u.	10su		a.u.	10su	a.u.	10su
α_{xx}	295.1962	$4.3689\ 10^{-23}$	300.0919	$4.44136\ 10^{-23}$	β_{xxx}	1361.0509	$1.176\ 10^{-26}$	1168.6394	$1.010\ 10^{-26}$
α_{xy}	21.3096	$3.15382\ 10^{-24}$	17.1894	$2.54404\ 10^{-24}$	β_{yyy}	629.0165	$5.435\ 10^{-27}$	678.6820	$5.864\ 10^{-27}$
α_{yy}	247.9879	$3.67022\ 10^{-23}$	246.3712	$3.64629\ 10^{-23}$	β_{zzz}	64.0711	$5.536\ 10^{-28}$	115.0256	$9.939\ 10^{-28}$
α_{xz}	-1.6823	$-2.48973\ 10^{-25}$	-5.0579	$-7.48564\ 10^{-25}$	β_{xyy}	99.1715	$8.569\ 10^{-28}$	79.8112	$6.896\ 10^{-28}$
α_{yz}	-9.6889	$-1.43395\ 10^{-24}$	-5.6495	$-8.36127\ 10^{-25}$	β_{xxy}	-259.0794	$-2.239\ 10^{-27}$	-305.8531	$-2.643\ 10^{-27}$
α_{zz}	182.0219	$2.69392\ 10^{-23}$	184.0875	$2.72449\ 10^{-23}$	β_{xxz}	-56.7604	$-4.905\ 10^{-28}$	-104.8374	$-9.059\ 10^{-28}$
Δ_α	188.1646	$2.78484\ 10^{-23}$	187.8842	$2.78069\ 10^{-23}$	β_{xzz}	-14.7152	$-1.272\ 10^{-28}$	-29.8526	$-2.580\ 10^{-28}$
μ_x	-0.6460	$-9.5608\ 10^{-26}$	-1.7901	$-2.6494\ 10^{-25}$	β_{yzz}	2.9027	$2.508\ 10^{-29}$	-3.9535	$-3.416\ 10^{-29}$
μ_y	-0.3151	$-4.6641\ 10^{-26}$	-0.6982	$-1.0334\ 10^{-25}$	β_{yyz}	19.0683	$1.648\ 10^{-28}$	6.7334	$5.818\ 10^{-29}$
μ_z	0.7447	$1.10222\ 10^{-25}$	0.4919	$7.28012\ 10^{-26}$	β_{total}	1493.0494	$1.290\ 10^{-26}$	1273.3171	$1.100\ 10^{-26}$
μ_g	1.0350		1.9834						
	FC7		**FC8**			**FC7**		**FC8**	
	a.u.	10su	a.u.	10su		a.u.	10su	a.u.	10su
α_{xx}	327.3890	$4.84536\ 10^{-23}$	320.3554	$4.74126\ 10^{-23}$	β_{xxx}	-1361.0752	$-1.176\ 10^{-26}$	1367.2541	$1.181\ 10^{-26}$
α_{xy}	1.7492	$2.58876\ 10^{-25}$	12.8487	$1.90161\ 10^{-24}$	β_{yyy}	-560.6658	$-4.845\ 10^{-27}$	639.1056	$5.523\ 10^{-27}$
α_{yy}	256.5072	$3.79631\ 10^{-23}$	259.4444	$3.83978\ 10^{-23}$	β_{zzz}	207.4260	$1.792\ 10^{-27}$	158.2692	$1.368\ 10^{-27}$
α_{xz}	7.1088	$1.0521\ 10^{-24}$	-2.9214	$-4.32365\ 10^{-25}$	β_{xyy}	-85.6577	$-7.402\ 10^{-28}$	70.1283	$6.060\ 10^{-28}$
α_{yz}	10.7504	$1.59106\ 10^{-24}$	-7.7691	$-1.14983\ 10^{-24}$	β_{xxy}	-441.6346	$-3.816\ 10^{-27}$	-316.2110	$-2.732\ 10^{-27}$
α_{zz}	190.8713	$2.8249\ 10^{-23}$	192.4431	$2.84816\ 10^{-23}$	β_{xxz}	-36.5550	$-3.159\ 10^{-28}$	-124.6807	$-1.077\ 10^{-27}$
Δ_α	195.2151	$2.88918\ 10^{-23}$	197.5495	$2.92373\ 10^{-23}$	β_{xzz}	-32.2150	$-2.784\ 10^{-28}$	2.0534	$1.774\ 10^{-29}$
μ_x	2.5444	$3.7657\ 10^{-25}$	-2.5888	$-3.8314\ 10^{-25}$	β_{yzz}	-5.7377	$-4.958\ 10^{-29}$	15.8893	$1.373\ 10^{-28}$
μ_y	0.9871	$1.4610\ 10^{-25}$	-0.3004	$-4.4459\ 10^{-26}$	β_{yyz}	1.5808	$1.366\ 10^{-29}$	0.1499	$1.296\ 10^{-30}$
μ_z	0.4343	$6.42805\ 10^{-26}$	1.3560	$2.00691\ 10^{-25}$	β_{total}	1798.1010	$1.554\ 10^{-26}$	1479.1511	$1.278\ 10^{-26}$

μ_g	2.7635		2.9378						

	FC9		FC10			FC9		FC10	
	a.u.	10su	a.u.	10su		a.u.	10su	a.u.	10su
α_{xx}	287.6813	4.25768 10^{-23}	270.2433	4.3929 10^{-23}	β_{xxx}	-1517.1837	-1.311 10^{-26}	-1892.8041	2.700 10^{-28}
α_{xy}	-3.6439	-5.39293 10^{-25}	0.8567	6.27352 10^{-25}	β_{yyy}	160.2992	1.385 10^{-27}	-189.6144	-1.027 10^{-27}
α_{yy}	217.8786	3.2246 10^{-23}	199.6236	2.85837 10^{-23}	β_{zzz}	176.4142	1.524 10^{-27}	245.7567	1.230 10^{-27}
α_{xz}	-4.9522	-7.32925 10^{-25}	12.2006	-2.2239 10^{-24}	β_{xyy}	96.4237	8.332 10^{-28}	-137.9156	-5.350 10^{-28}
α_{yz}	11.7588	1.7403 10^{-24}	14.5114	6.25485 10^{-25}	β_{xxy}	201.6752	1.743 10^{-27}	-321.3783	7.794 10^{-28}
α_{zz}	169.2348	2.50467 10^{-23}	167.8848	2.39383 10^{-23}	β_{xxz}	43.7127	3.777 10^{-28}	103.7977	-4.589 10^{-28}
Δ_α	167.3053	2.47612 10^{-23}	164.7299	2.438 10^{-23}	β_{xzz}	38.8611	3.358 10^{-28}	-66.3821	2.054 10^{-29}
μ_x	0.9361	1.3855 10^{-25}	0.8675	1.8356 10^{-25}	β_{yzz}	40.6738	3.515 10^{-28}	27.7781	-7.168 10^{-30}
μ_y	-1.0739	-1.5894 10^{-25}	1.0688	1.1403 10^{-26}	β_{yyz}	-21.0957	-1.823 10^{-28}	-5.3467	3.513 10^{-29}
μ_z	-0.7179	-1.06244 10^{-25}	0.8827	3.2421 10^{-26}	β_{total}	1453.0600	1.256 10^{-26}	-1892.8041	2.700 10^{-28}
μ_g	1.5953		1.2618						

To analyze the NLO parameters in Table 6, we compared the total second-order polarizability (βtot) and dipole moment (μtot) values of the compounds. βtot is an important parameter that determines the second-order optical response of the molecule, and higher values indicate that it can be a better NLO material.

The highest βtot value was calculated for FC9 and FC10 compounds with 1892.80418 a.u. The lowest βtot value belongs to FC2 compound with 944.20197 a.u. In general, FC9 and FC10 are seen to be the best NLO candidates.

When evaluated in terms of dipole moment, the highest dipole moment was in FC6 compound and was calculated as 1.98342 Debye. The lowest dipole moment was in FC2 compound with 1.16810 Debye. In general, it was found that FC6 was the compound with the highest values in terms of polarity.

Based on these data, the strongest NLO candidates in terms of βtot are FC9 and FC10. FC6 has the highest dipole moment and may be advantageous for NLO systems requiring high polarity. FC2 has the lowest values in terms of both βtot and μtot, and may have low NLO performance. This analysis helps to determine the most suitable compounds for optoelectronic and NLO applications.

4. Conclusions

In this study, the structural, electronic and optical properties of ferrocene-derived chalcone compounds were investigated in detail using density functional theory (DFT). Calculations were performed using the M06-2X functional and the 6-31+G(d)/LANL2DZ basis set, and the molecular reactivity, stability and possible biological interactions of the compounds were evaluated. While the HOMO-LUMO energy levels showed the synergistic interaction of ferrocene and chalcone units, the wide energy range revealed that the compounds had high stability. Molecular electrostatic potential (MEP) maps showed that these compounds could bind to biological targets via electrostatic interactions.

IR and UV-Vis spectra revealed that the compounds preserved their conjugation structures and were promising in terms of optical properties. In non-linear optical (NLO) analyses, it was determined that especially FC9 and FC10 compounds had high polarizability values and it was seen that these compounds could be suitable candidates for optoelectronic applications.

In general, the calculated molecular properties of ferrocene derived chalcone compounds indicate that these compounds have potential in pharmaceutical, biosensor and optoelectronic fields. In the future, it is suggested to verify their biological activities by experimental studies and design new derivatives.

ACKNOWLEDGEMENT

The numerical calculations reported in this paper were fully/partially performed at TUBITAK ULAKBIM, High Performance and Grid Computing Center (TRUBA resources). "Synthesis of Ferrocenyl-Containing Chalcone and Isoxazole Compounds and Investigation of Their Structural, Electronic and Anticancer Properties" was produced from Gamze TÜZÜN's doctoral thesis with this title.

Conflict of interest

The author has no relevant financial or nonfinancial interests to disclose.

Funding Declaration

This manuscript has no funding

References

[1] Kealy, T. J., & Pauson, P. L. A new type of organo-iron compound. Nature, 168(4285) (1951) 1039-1040.

[2] Larik, F. A., Saeed, A., Fattah, T. A., Muqadar, U., & Channar, P. A. Recent advances in the synthesis, biological activities and various applications of ferrocene derivatives. Applied Organometallic Chemistry, 31(8) (2017) e3664.

[3] Dickinson, B. C., & Chang, C. J. Chemistry and biology of reactive oxygen species in signaling or stress responses. Nature chemical biology, 7(8) (2011) 504-511.

[4] Okolo, E. N., Ugwu, D. I., Ezema, B. E., Ndefo, J. C., Eze, F. U., Ezema, C. G., ... & Ujam, O. T. New chalcone derivatives as potential antimicrobial and antioxidant agent. Scientific reports, 11(1) (2021) 21781.

[5] Rauf, U., Shabir, G., Bukhari, S., Albericio, F., & Saeed, A. Contemporary developments in ferrocene chemistry: physical, chemical, biological and industrial aspects. Molecules, 28(15) (2023) 5765.

[6] Gordon, E. M., Barrett, R. W., Dower, W. J., Fodor, S. P., & Gallop, M. A. Applications of combinatorial technologies to drug discovery. 2. Combinatorial organic synthesis, library screening strategies, and future directions. Journal of medicinal chemistry, 37(10) (1994) 1385-1401.

[7] Honarparvar, B., Govender, T., Maguire, G. E., Soliman, M. E., & Kruger, H. G. Integrated approach to structure-based enzymatic drug design: molecular modeling, spectroscopy, and experimental bioactivity. Chemical reviews, 114(1) (2014) 493-537.

[8] Dennington, R., Keith, T. A., & Millam, J. M. (2016). GaussView 6.0. 16. Semichem Inc.: Shawnee Mission, KS, USA.

[9] Frisch M.J., Trucks G.W., Schlegel H.B., Scuseria G.E., Robb M.A., Cheeseman J.R., Scalmani G., Barone V., Mennucci B., Petersson G.A., Nakatsuji H., Caricato M., Li X., Hratchian H.P., Izmaylov A.F., Bloino J., Zheng G., Sonnenberg J.L., Hada M., Ehara M., Toyota K., Fukuda R., Hasegawa J., Ishida M., Nakajima T., Honda Y., Kitao O., Nakai H., Vreven T., Montgomery J.A., Peralta J.E., Ogliaro F., Bearpark M., Heyd J.J., Brothers E., Kudin K.N., Staroverov V.N., Kobayashi R., Normand J., Raghavachari K., Rendell A., Burant J.C., Iyengar S.S., Tomasi J., Cossi M., Rega N., Millam J.M., Klene M., Knox J.E., Cross J.B., Bakken V., Adamo C., Jaramillo J., Gomperts R., Stratmann R.E., Yazyev O., Austin A.J., Cammi R., Pomelli C., Ochterski J.W., Martin R.L., Morokuma K., Zakrzewski V.G., Voth G.A., Salvador P., Dannenberg J.J., Dapprich S., Daniels A.D., Farkas O., Foresman J.B., Ortiz J.V., Cioslowski J.,Fox D.J. (2009) Gaussian 09, revision D.01. Gaussian Inc, Wallingford CT

[10] Tapera, M., Kekeçmuhammed, H., Tüzün, B., Daştan, S. D., Çelik, M. S., Taslimi, P., ... & Sarıpınar, E. Novel 1, 2, 4-triazole-maleamic acid derivatives: Synthesis and evaluation as anticancer agents with carbonic anhydrase inhibitory activity. Journal of Molecular Structure, 1313 (2024) 138680.

[11] Karimi, S., Mafton-Azad, L., Behnajady, B., & Tüzün, B. Response Surface Methodology (RSM) Design to Optimize the Cathode of Li-Ions Batteries Recycling in Deep Eutectic Solvent and DFT

Simulation. Korean Journal of Chemical Engineering, 42(2)(2025) 361-381.

[12] Waleed Shinwari, M., Jamal Deen, M., Starikov, E. B., & Cuniberti, G. Electrical conductance in biological molecules. Advanced Functional Materials, 20(12) (2010) 1865-1883.

[13] Ayalew, M. E. DFT studies on molecular structure, thermodynamics parameters, HOMO-LUMO and spectral analysis of pharmaceuticals compound quinoline (Benzo [b] Pyridine). Journal of Biophysical Chemistry, 13(3) (2022) 29-42.

[14] Ayalew, M. E. DFT studies on molecular structure, thermodynamics parameters, HOMO-LUMO and spectral analysis of pharmaceuticals compound quinoline (Benzo [b] Pyridine). Journal of Biophysical Chemistry, 13(3) (2022) 29-42.

[15] Choudhary, V., Bhatt, A., Dash, D., & Sharma, N. DFT calculations on molecular structures, HOMO–LUMO study, reactivity descriptors and spectral analyses of newly synthesized diorganotin (IV) 2-chloridophenylacetohydroxamate complexes. Journal of computational chemistry, 40(27) (2019) 2354-2363.

[16] Mumit, M. A., Pal, T. K., Alam, M. A., Islam, M. A. A. A. A., Paul, S., & Sheikh, M. C. DFT studies on vibrational and electronic spectra, HOMO–LUMO, MEP, HOMA, NBO and molecular docking analysis of benzyl-3-N-(2, 4, 5-trimethoxyphenylmethylene) hydrazinecarbodithioate. Journal of molecular structure, 1220 (2020) 128715.

[17] Sworakowski, J. How accurate are energies of HOMO and LUMO levels in small-molecule organic semiconductors determined from cyclic voltammetry or optical spectroscopy?. Synthetic Metals, 235 (2018) 125-130.

[18] Demircioğlu, Z., Kaştaş, Ç. A., & Büyükgüngör, O. Theoretical analysis (NBO, NPA, Mulliken Population Method) and molecular orbital studies (hardness, chemical potential, electrophilicity and Fukui function analysis) of (E)-2-((4-hydroxy-2-methylphenylimino) methyl)-3-methoxyphenol. Journal of Molecular structure, 1091 (2015) 183-195.

[19] Fatima, Q., Zhang, H., Haidry, A. A., Hussain, R., Alshgari, R. A., & Mohammad, S. Elucidating the optoelectronic properties Ag, Au and Pd doped graphene oxide using a DFT approach. Diamond and Related Materials, 146 (2024) 111151.

[20] Chen, X., Yan, C. C., Zhang, X., Zhang, X., Dai, F., Yin, J., & Zhang, Y. Drug–target interaction prediction: databases, web servers and computational models. Briefings in bioinformatics, 17(4) (2016) 696-712.

[21] Kumar, S. Spectroscopy of organic compounds. Cosmic rays, 10(4) (2006).

[22] Birge, R. R. Photophysics and molecular electronic applications of the rhodopsins. Annual review of physical chemistry, 41(1) (1990) 683-733.

SUPPLEMENTARY DATA

INVESTIGATION OF STRUCTURAL PROPERTIES OF FERROCENE-DERIVED CHALCONE COMPOUNDS

Gamze Tüzün, Koray Sayın

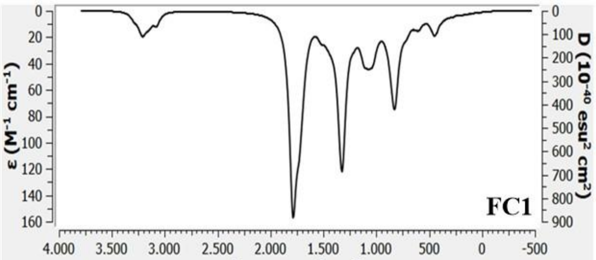

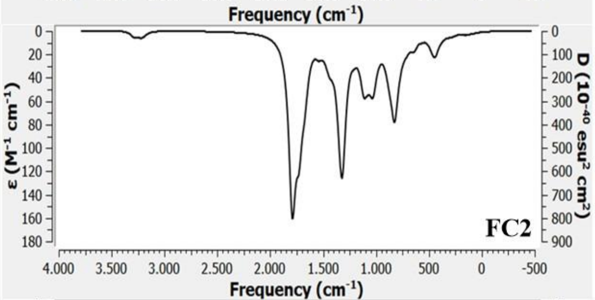

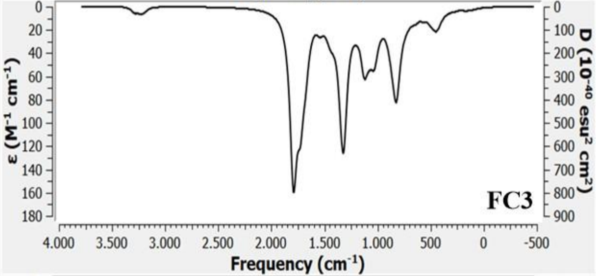

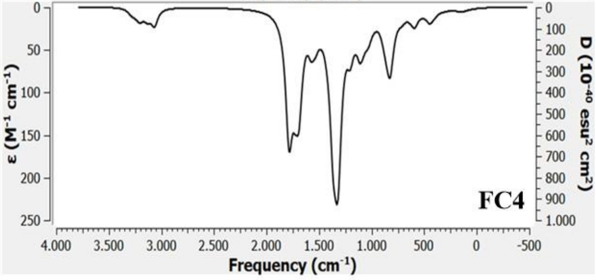

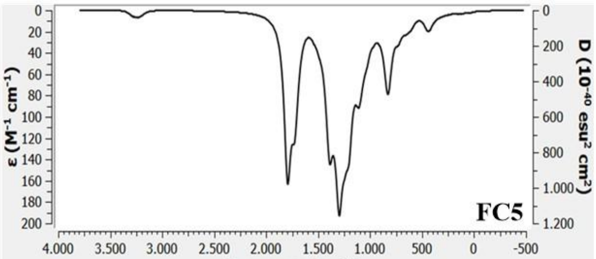

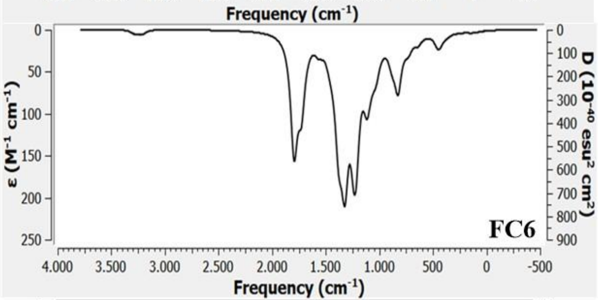

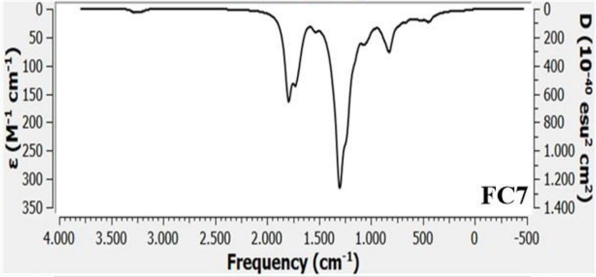

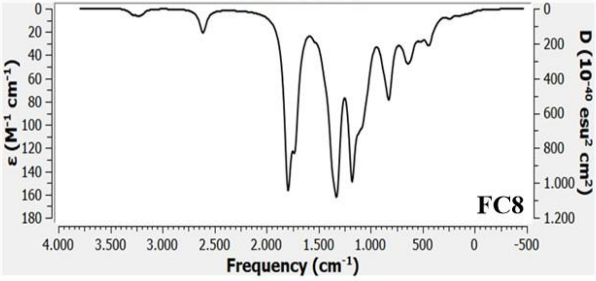

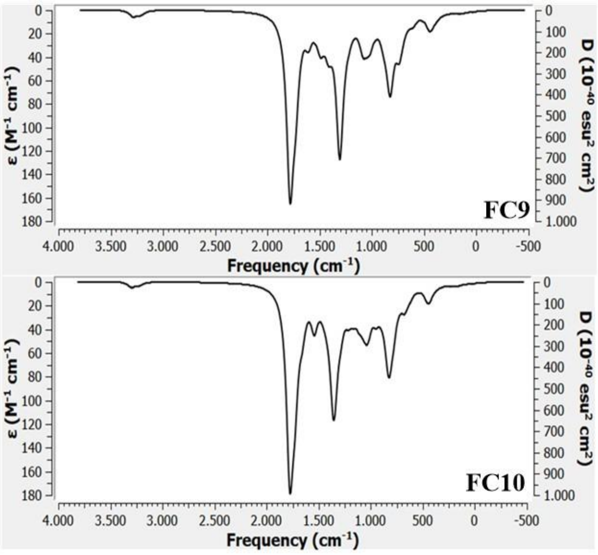

Figure S1. IR spectra of ferrocene-based chalcone derivative molecules

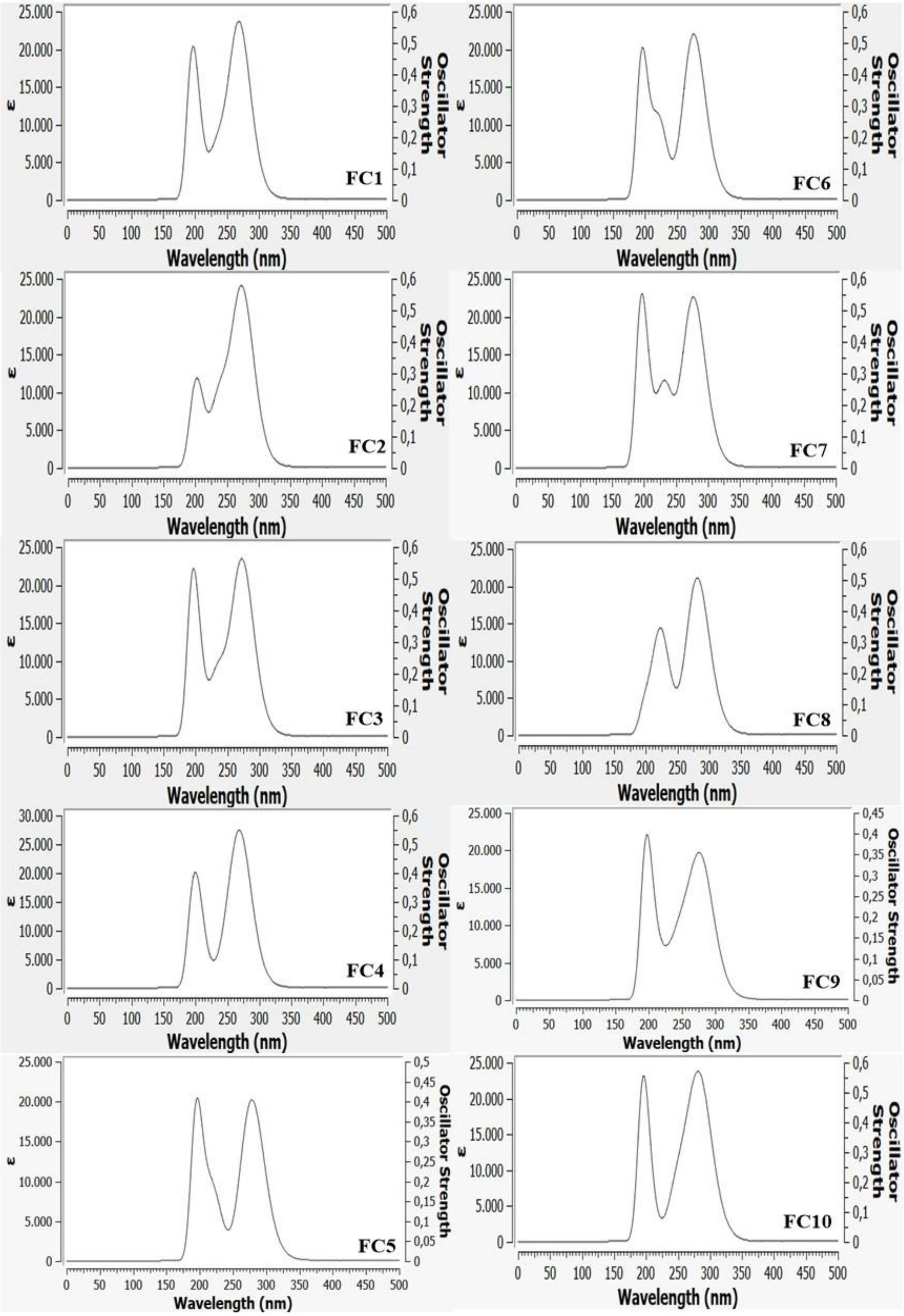

Figure S2. UV-Vis spectra of ferrocene-based chalcone derivative molecules